J. Cent. South Univ. (2013) 20: 791–798
DOI: 10.1007/s11771-013-1550-7

Springer

Stereo particle image velocimetry measurement of 3D soil deformation around laterally loaded pile in sand

YUAN Bing-xiang(袁炳祥)[1,2], CHEN Wen-wu(谌文武)[1,2], JIANG Tong(姜彤)[3],
WANG Yi-xian(汪亦显)[4], CHEN Ke-ping(陈科平)[4]

1. Key Laboratory of Mechanics on Disaster and Environment in Western China (Ministry of Education), Lanzhou University, Lanzhou 730000, China;
2. School of Civil Engineering and Mechanics, Lanzhou University, Lanzhou 730000, China;
3. North China University of Water Resources and Electric Power, Zhengzhou 450011, China;
4. School of Resources and Safety Engineering, Central South University, Changsha 410083, China

Abstract: A developed stereo particle image velocimetry (stereo-PIV) system was proposed to measure three-dimensional (3D) soil deformation around a laterally loaded pile in sand. The stereo-PIV technique extended 2D measurement to 3D based on a binocular vision model, where two cameras with a well geometrical setting were utilized to image the same object simultaneously. This system utilized two open software packages and some simple programs in MATLAB, which can easily be adjusted to meet user needs at a low cost. The failure planes form an angle with the horizontal line, which are measured at 27°–29°, approximately three-fourths of the frictional angle of soil. The edge of the strain wedge formed in front of the pile is an arc, which is slightly different from the straight line reported in the literature. The active and passive influence zones are about twice and six times of the diameter of the pile, respectively. The test demonstrates the good performance and feasibility of this stereo-PIV system for more advanced geotechnical testing.

Key words: particle image velocimetry; digital image correlation; stereo particle image velocimetry; laterally loaded pile; scaled model; 3D soil deformation; soil-structural interaction

1 Introduction

Particle image velocimetry (PIV) was an optical method to measure instantaneous flow displacement vectors by tracking seeded particle movement. The PIV technique was well known as different names in other fields, such as digital image correlation (DIC), surface displacement measurement, and computer vision. The PIV technique was to obtain two-dimensional (2D) displacement field by correlating two consecutive images. Because of its simple implementation, PIV had been used in many fields after its first application reported in 1980s [1]. At present, PIV is utilized in various fields, including aerospace engineering [2], biology [3–4], and geotechnical engineering [5–8].

Stereo particle image velocimetry (stereo-PIV) was a more advanced optical measurement method compared with traditional PIV. This technique can overcome the limitation of the traditional PIV, which can only provide planar information. The stereo-PIV technique was developed to measure three-dimensional (3D) deformation using two cameras instead of one camera in a regular PIV system. However, limited case studies of stereo-PIV applications had been reported in geotechnical engineering because of its complicated implementation. TAYLOR et al [9] used a method similar to stereo-PIV to determine planar and 3D deformation induced by tunneling through tracking target markers embedded in clay. VIKRANT et al [10] used this technique to quantify dynamic specimen 3D response during buried blast loading.

The pile foundation not only transmitted vertical loads to the soil, but also resisted horizontal loads in the soil. The problem of a laterally loaded pile had been investigated for more than a half century. Many methods such as BROMS' method [11], the *p-y* curve approach [12], and the strain wedge method [13], had been developed to analyze the laterally loaded pile. All these methods were adopted to simplify heterogeneous characteristics of soil and non-linear soil–pile interaction. Additionally, these methods focused on the load and

Foundation item: Project(104244) supported by the Natural Sciences and Engineering Research Council of Canada
Received date: 2011–11–24; **Accepted date:** 2012–04–10
Corresponding author: CHEN Wen-wu, Professor, PhD; Tel: +86–18929374897; E-mail: bingxiangyuan@gmail.com

deformation relationship of the pile where only limited information was available on soil surface movement around the pile. The field experiments may be considered as the best way to provide exact soil deformation around a pile under lateral load. However, these field experiments needed high costs for experimental setup and labor.

A scaled model test was presented to measure the 3D soil deformation on the ground surface around a laterally loaded pile in sand using an in-house developed stereo-PIV system. The stereo-PIV system utilized two open software packages composed of some simple programs in MATLAB. This developed system can be easily adjusted to meet researcher needs at a much lower costs as compared with commercially available systems. The displacement and strain fields were obtained through the model test using the stereo-PIV system. This simple test demonstrated the good performance of this system for more advanced geotechnical laboratory testing.

2 Principle of stereo-PIV

Visualization and quantification of soil deformation may be considered as the best way to understand geotechnical engineering problems. The PIV technique had been used to visualize and quantify soil deformation. This technique was a classic pattern recognition technique where two consecutive images were correlated to obtain the particle displacement vectors. The stereo-PIV technique was a developed optical measurement technique based on the PIV technique and a binocular vision model. Two cameras were set up in different locations to capture images, from which the 3D displacement field was calculated.

2.1 Particle image velocimetry

The PIV technique was to divide the entire image area into many smaller interrogation windows, and to correlate these interrogation windows to obtain the displacement vector of each interrogation window. In this technique, a cross-correlation method was used to match each interrogation window. The standard cross-correlation function of two continuous real functions $h(m, n)$ and $g(m, n)$, denoted as L, was defined as

$$L(\Delta m,\Delta n)=\iint_A h(m,n)g(\Delta m+m,\Delta n+n)\mathrm{d}m\mathrm{d}n \quad (1)$$

where m and n are dimensions of the interrogated images; h and g are gray scale intensities of the two images being interrogated.

The cross-correlation function was applied repeatedly while shifting the images by distances Δm and Δn. If $L(\Delta m, \Delta n)$ had a peak value, then the best match of $h(m, n)$ and $g(m, n)$ occurred when $g(m, n)$ was shifted by the distances Δm and Δn. More details of the correlation function of the PIV technique can be found in Refs. [14–15].

2.2 Calibration of cameras' parameters

In the stereo-PIV system, two cameras were utilized to capture images based on a binocular vision model. In order to contain 3D deformation from the paired images by the two cameras, the parameters of each camera were needed to calibrate with respect to the region of interest (ROI). A series of paired pictures, which were simultaneously taken by the two cameras, were used to calibrate the camera parameters. There were three coordinate systems, the image coordinate system (x, y), the left and right camera coordinate systems (X_l, Y_l, Z_l) and (X_r, Y_r, Z_r), and the global coordinate system (X_w, Y_w, Z_w), which were important to calculate the cameras' parameters, as shown in Fig. 1. The point P in the global coordinate system was separately projected to two points PR and PL onto the right and left camera images. The point mapping relationship between the image coordinate and the global coordinate can be described in the following equation:

$$Z_l\begin{bmatrix}x\\y\\1\end{bmatrix}=\begin{bmatrix}f_x & 0 & x_0 & 0\\0 & f_y & y_0 & 0\\0 & 0 & 1 & 0\end{bmatrix}\begin{bmatrix}r_{11} & r_{12} & r_{13} & t_1\\r_{21} & r_{22} & r_{23} & t_2\\r_{31} & r_{33} & r_{33} & t_3\\0 & 0 & 0 & 1\end{bmatrix}\begin{bmatrix}X_w\\Y_w\\Z_w\\1\end{bmatrix} \quad (2)$$

where f_x and f_y are the focal lengths in pixels along the X and Y axes; (x_0, y_0) are the coordinates of the principal point; $\boldsymbol{R}=r_{11}, \cdots, r_{33}$, is the rotation matrix; $\boldsymbol{T}=t_1, t_2, t_3$, is the translation vector.

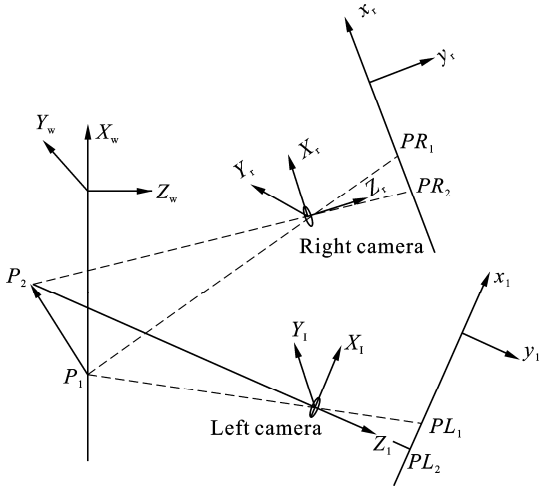

Fig. 1 Sketch of coordinate systems

The focal lengths, principal point coordinates, rotation matrix, and the translation vector of each camera system were calculated using Eq. (2), the known global coordinates, and image coordinates, which were

provided by a series of images.

2.3 Composition of 3D displacement field

Composition of 3D displacement vectors utilized the parameters of the two cameras and the corresponding 2D displacement vector pairs. One particle movement in the global coordinate system was separately projected to two 2D movements onto the left and right camera images. On the contrary, the image coordinates of the two paired points can determine the global coordinate of the particle. ZHANG and YAU [16] used a similar method to construct 3D shapes with two cameras. By combining Eq. (2) of the two-camera system, the global coordinate (X_w, Y_w, Z_w) of the particle can be calculated as

$$\begin{bmatrix} \Delta x^l r_{31}^l - f_x^l r_{11}^l & \Delta x^l r_{32}^l - f_x^l r_{12}^l & \Delta x^l r_{33}^l - f_x^l r_{13}^l \\ \Delta y^l r_{31}^l - f_y^l r_{21}^l & \Delta y^l r_{32}^l - f_y^l r_{22}^l & \Delta y^l r_{33}^l - f_y^l r_{23}^l \\ \Delta x^r r_{31}^r - f_x^r r_{11}^r & \Delta x^r r_{32}^r - f_x^r r_{12}^r & \Delta x^r r_{33}^r - f_x^r r_{13}^r \\ \Delta y^r r_{31}^r - f_y^r r_{21}^r & \Delta y^r r_{32}^r - f_y^r r_{22}^r & \Delta y^r r_{33}^r - f_y^r r_{23}^r \end{bmatrix} \cdot \begin{bmatrix} X_w \\ Y_w \\ Z_w \end{bmatrix} = \begin{bmatrix} f_x^l t_1^l - \Delta x^l t_3^l \\ f_y^l t_2^l - \Delta y^l t_3^l \\ f_x^r t_1^r - \Delta x^r t_3^r \\ f_y^r t_1^r - \Delta y^r t_3^r \end{bmatrix} \tag{3}$$

$$\Delta x = (x - x_0)\{1 + k_1\left[(x - x_0)^2 / f_x^2 + (y - y_0)^2 / f_y^2\right] + k_2\left[(x - x_0)^2 / f_x^2 + (y - y_0)^2 / f_y^2\right]^2\} \tag{4}$$

$$\Delta y = (y - y_0)\{1 + k_1\left[(x - x_0)^2 / f_x^2 + (y - y_0)^2 / f_y^2\right] + k_2\left[(x - x_0)^2 / f_x^2 + (y - y_0)^2 / f_y^2\right]^2\} \tag{5}$$

where superscript "l" and "r" represent the parameters from the left and right cameras; and k_1 and k_2 are the image distortion coefficients, which were obtained in the first step.

During the particle movement from (X_w^1, Y_w^1, Z_w^1), to (X_w^2, Y_w^2, Z_w^2), the displacement vector (U, V, W) of the particle was calculated as

$$\begin{bmatrix} U \\ V \\ W \end{bmatrix} = \begin{bmatrix} X_w^2 \\ Y_w^2 \\ Z_w^2 \end{bmatrix} - \begin{bmatrix} X_w^1 \\ Y_w^1 \\ Z_w^1 \end{bmatrix} \tag{6}$$

3 Experimental setup and procedures

3.1 Developed experimental setup

The optical test setup included two complementary metal-oxide-semiconductor (CMOS) cameras, a load cell, a linear differential variable transformer (LDVT), a loading frame, an acrylic model pile, and a computer, as shown in Fig. 2. The cameras had a resolution of 1 280× 1 024 pixels. They were controlled to synchronously capture images by an in-house developed software driver using MATLAB commands. The time difference between two cameras was limited to 0.1 s. The load cell and LDVT were utilized to measure the lateral loads and pile movements of the pile laterally loaded. The data were acquired by a developed data acquisition (DAQ) system, which included a NI-6011E PC card, a SCB-68 shielded connector and an in-house developed driver in LabView. The Plexiglas mould had dimensions of 220 mm (wide)×420 mm (long)×310 mm (height). An acrylic model pile with a diameter of 14.5 mm and a length of 150 mm was used in this work. A black and white grid patterns with grid spacing of 20 mm was printed for calibration of the cameras' parameters. The loose sand with a dry unit weight of 14.86 kN/m^3 was used in this work. The friction angle of loose sand was measured at 38.4° through direct shear tests.

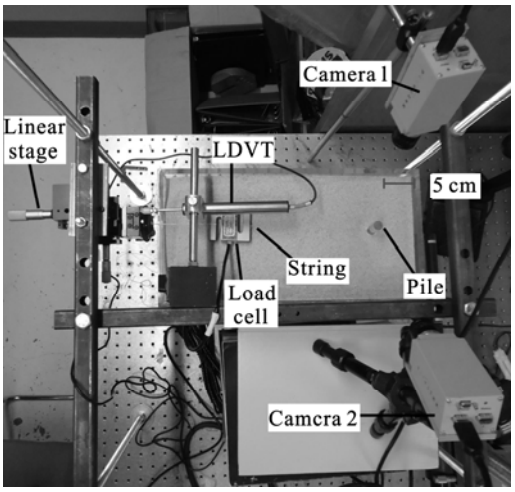

Fig. 2 Experimental setup

3.2 Experimental procedures

The first step was to calibrate the parameters of two cameras. The two cameras were set up in two optimal locations in order to have a large common field. The black and white grid pattern with grid spacing of 20 mm was printed and pasted on a flat and thin panel. The panel was targeted on the sand surface and a pair of pictures was taken from the two cameras. The two pictures were named C11 and C21. By changing the panel positions, another three pairs of pictures of the panel, shown in Fig. 3, were obtained to calculate the parameters of the cameras. The camera calibration toolbox for MATLAB [17] was used to calibrate the camera system in this work. This toolbox included reading images, extracting the grid corners, calibration, and analyzing reprojection error. When extracting the grid corners, it was important to determine the clicking order. More details can be found on their webpage [17]. Through this calibration

procedure, the focal lengths, principal point coordinates, distortion coefficients, rotation matrix, and the translation vector of each camera were obtained.

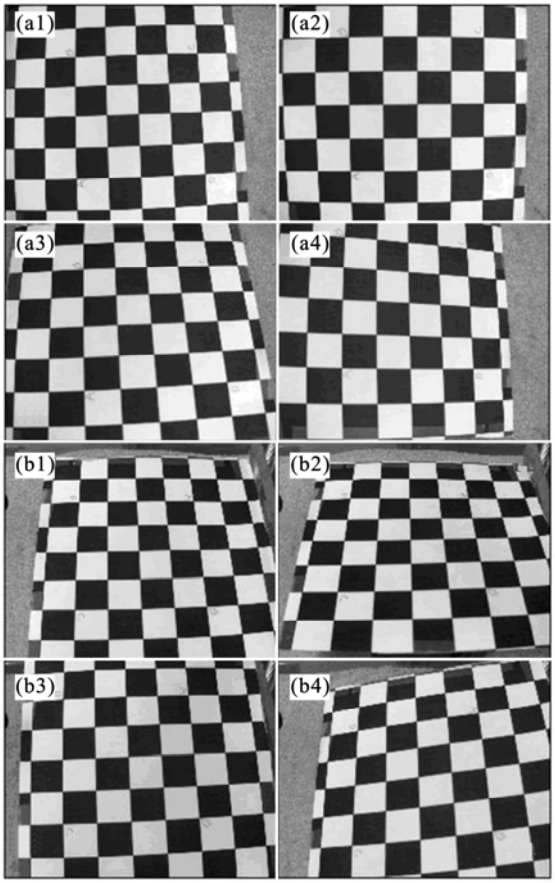

Fig. 3 Four pairs of pictures taken by left and right cameras: (a1−a4) Four pictures taken by left camera; (b1−b4) Four pictures taken by right camera

The second step was to capture a series of paired soil images and to calculate the 2D displacement vectors. The model pile was embedded 120 mm deep and located about 30 mm above the sand surface. The pile was connected to the loading frame through a string at the loading point, which was about 10 mm below the pile head, as shown in Fig. 2. The load was applied through a screw mechanism by manually rotating a handle. The load cell and LDVT were used to measure the load and deformation at the loading point. The load versus displacement curve is shown in Fig. 4. The 2D displacement vectors were calculated through two consecutive images by the demo PIVview2C analysis software [18], as shown in Fig. 5. This software had features to allow users to select the window size, correlation algorithm, peak detection, etc. Through this image correlation procedure, the 2D displacement vectors of the left and right cameras were obtained.

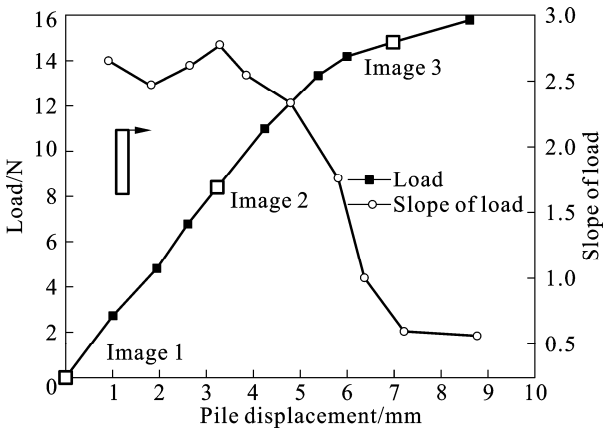

Fig. 4 Load and slope of load versus displacement curves from model pile

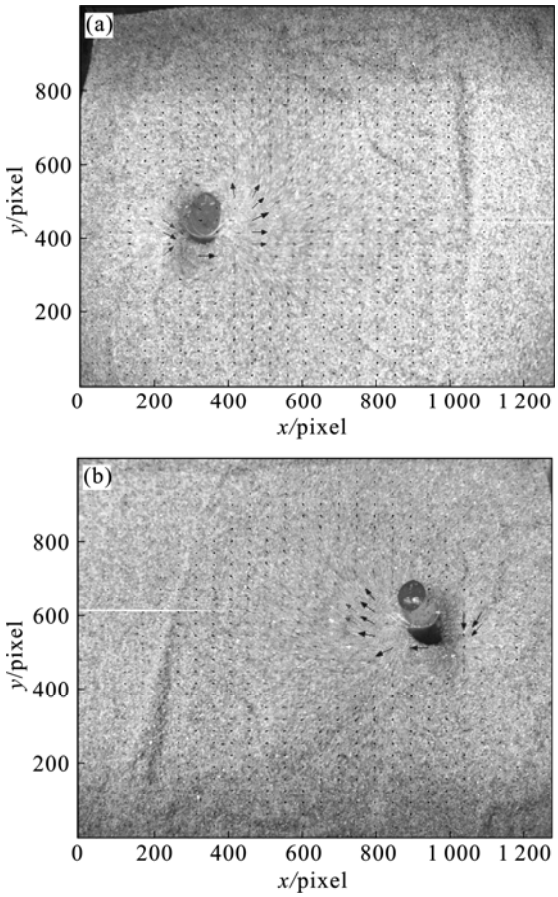

Fig. 5 2D displacement vectors calculated by PIVview2C: (a) 2D displacement vectors in left camera (b) 2D displacement vectors in right camera

The last step was to reconstruct the 3D displacement field using the parameters of two cameras calculated in the first step and the corresponding planar displacement vector pairs from the second step. One particle in the global coordinate system was separately projected to two points onto the left and right camera images. Inversely, the image coordinates of the two points can determine the global coordinate of the particle.

The global coordinate of the particle can be calculated by Eq. (3). The global coordinates before and after deformation were separately calculated using the 2D coordinates. The 3D displacement vector was calculated by Eq. (6). Through this step, the 3D displacement vectors of the sand surface were obtained.

4 Results and analysis

4.1 Load versus displacement curve

The load and displacement of the model pile at the loading point were acquired during the whole test. The typical points captured during the pile movement were labeled in Fig. 4. The load versus displacement curve is similar to the typical curve reported for a laterally loaded pile in loose sand. The slope of load versus displacement curve, also shown in Fig. 4, represents the soil resistant behaviour under laterally loading. At the beginning, the load increases almost linearly with the pile displacement increasing, which represents the elastic behaviour of soil. The slope of load gradually decreases with increasing the displacement, which represents the plastic behaviour of soil.

4.2 Two-dimensional displacement field

The planar displacement field of the sand surface is the basic information to analyze the sand movement. The 2D displacement field can be calculated by setting up a camera, whose optical axis is perpendicular to the horizontal plane, using the PIV technique as well [19]. Figure 6 shows the planar displacement field at different loading stages. The first displacement field shown in Fig. 6(a) is between Images 1 and 2. The second displacement field shown in Fig. 6(b) is accumulated by two displacement fields: the first displacement field between Images 1 and 2, and the other between Images 2 and 3. It is assumed that superposition principle is applicable in this small displacement problem studied here. The horizontal displacement, U, is also shown in the contour in Fig. 6, whose shape resembles the contour lines from LIU et al [20]. As expected, the 2D displacement increases with the lateral pile movement. The displacement within the mobilized block implies a significant shearing occurring in the sand. The region mobilized by the pile movement is curved first from the edge of the pile.

4.3 Vertical displacement field

In addition to the 2D displacement field shown in Fig. 6, the vertical displacement, W, out of planar field, is also obtained by stereo-PIV. Figure 7 shows 3D view of the vertical displacement field at different loading stages: The first displacement field shown in Fig. 7(a) is between Images 1 and 2. The second displacement field

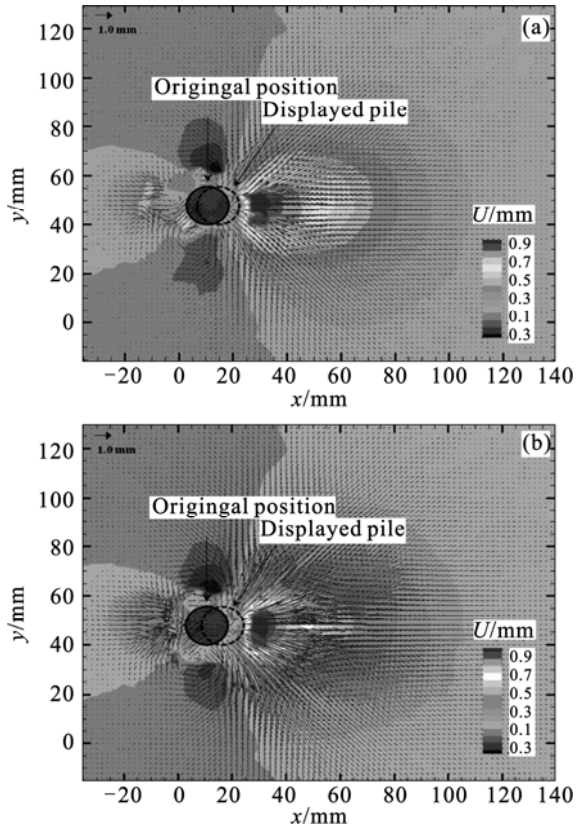

Fig. 6 2D soil displacement field at different loading stages: (a) 2D displacement field between Images 1 and 2; (b) 2D displacement field between Images 1 and 3

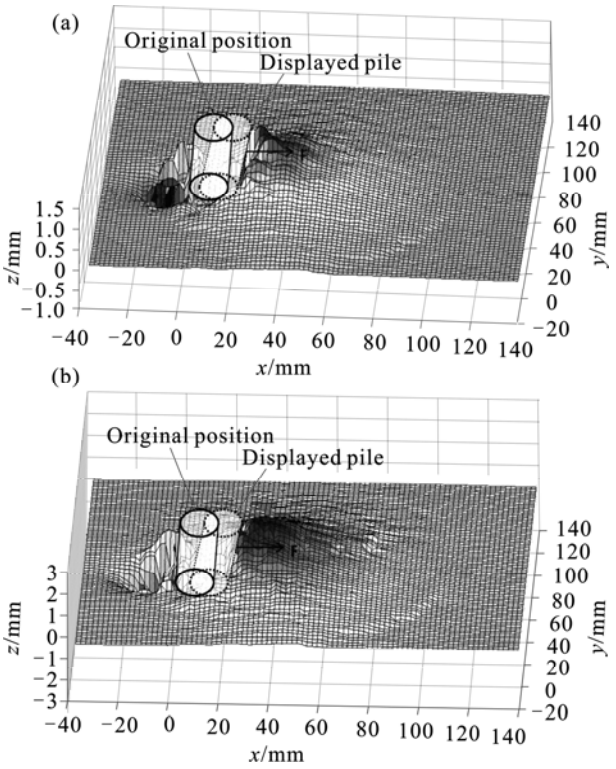

Fig. 7 3D view of vertical displacement field at different loading stages: (a) Vertical displacement field between Images 1 and 2; (b) Vertical displacement field between Images 1 and 3

shown in Fig. 7(b) is between Images 1 and 3. It is worth noting that there are some errors on vertical displacements around the pile head. The reason is that the displacements of the pile head are mistaken as the soil movement in this area from image processing by PIVview2C, which causes minor errors in the progress of composition of 3D displacements.

Figure 8 shows the contours of the vertical displacements at different loading stages of testing. The displacement field shown in Fig. 8(a) is between Images 1 and 2, and the displacement field shown in Fig. 8(b) is between Images 1 and 3. The planar displacements are represented by the vectors and the vertical displacements are represented by the color contours. As expected, the soil moved not only on the plane, but also in vertical direction during lateral pile movement. Figures 6 and 8 demonstrate that the passive influence zone ahead of the pile is larger than the active influence zone behind the pile.

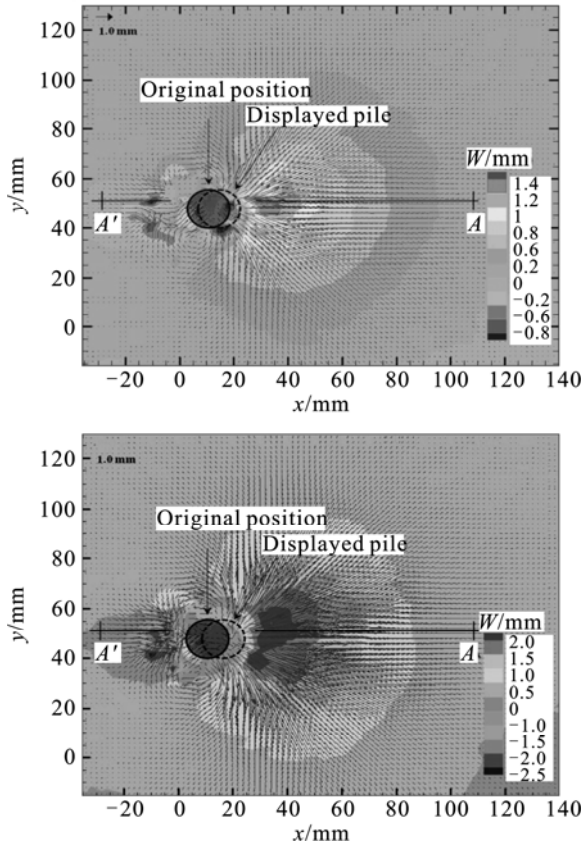

Fig. 8 Contours of vertical displacement field at different loading stages: (a) Contours of vertical displacement field between Images 1 and 2: (b) Contours of vertical displacement field between Images 1 and 3

4.4 Soil displacements along loading direction

In order to see the change of soil horizontal and vertical direction displacements along loading direction, U and W, the soil displacements curves along the section A–A' in Fig. 8 are shown in Fig. 9, where the distance from the pile center is normalized by the pile diameter. As expected, the soil displacements along loading direction and vertical direction both increase while the pile is pulled. The values of U and W between Images 1 and 2 are smaller than those between Images 1 and 3. From Fig. 9, it is also demonstrated that the position of the peak vertical displacement is almost coincident with that of the peak horizontal displacement. In the passive influence zone, the displacements decrease with the distance away from the pile after the peak value. Between Images 1 and 3, the most significant influence zone of the horizontal and vertical displacements is limited to a distance approximately six times the pile diameter from the pile center. Beyond this zone, the soil displacements are less than 10% of peak values, which are almost ignored. Based on Figs. 6–8, the active influence zone is only about twice the diameter of the pile; the passive influence zone is approximately six times the diameter of the pile.

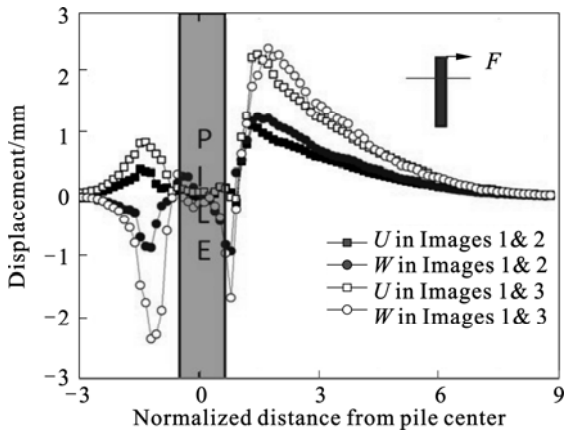

Fig. 9 Soil movement along section A–A' in Fig. 8

4.5 Shear strain field

The shear strain can be calculated from the planar displacements. A similar method had been used by other researchers [20]. The failure plane can be delineated by linking the maximum shear strain points, since soil normally fails by shearing. It is worth noting that the shear strain field, as shown in Fig. 10, corresponds to the displacement field in Fig. 6(b). It can be seen that the failure plane was almost linearly extended from the pile and formed a shear strain wedge. The straight lines can be used to delineate approximately the failure planes. The angles between the failure planes and the horizontal plane are measured at 27°–29°, which are approximately three-fourths of the internal friction angle of soil. The asymmetrical angles are caused by the test layout where the lateral force is applied with an angle from the horizontal plane.

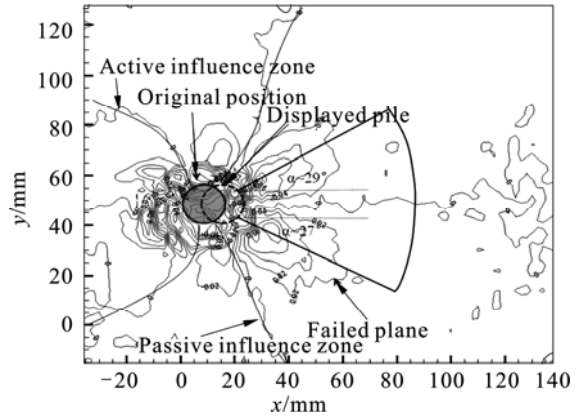

Fig. 10 2D shear strain field between Images 1 and 3

4.6 Change rate of vertical displacements

The change rate of vertical displacements is shown in Fig. 11, which is the subtraction between the vertical displacements of two adjacent points along the loading direction. It is demonstrated that the change rate of vertical displacements around the pile is larger than that in other place. With the distance away from the pile, the change rate decreased obviously. The change rate of vertical displacements was limited to a distance approximately six times the pile diameter ahead of the pile. Based on Figs. 8, 9, and 11, the edge of the strain wedge was an arc, as shown in Fig. 10, which is slightly different from the straight line as stated in previous work.

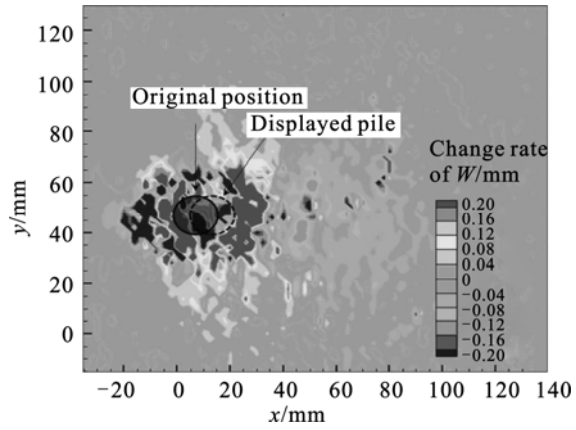

Fig. 11 Change rate of soil vertical displacements

5 Conclusions

1) A stereo-PIV system is developed to measure the soil displacement and shear strain fields around a laterally loaded pile. This system utilizes two open software packages and some simple programs in MATLAB, which can be easily adjusted to meet researcher needs at a lower cost.

2) The load versus displacement curve is similar to the typical load versus displacement curve for a laterally loaded pile in loose sand. The planar and vertical displacement fields are calculated during the pile laterally loading. The active influence zone is about twice the diameter of the pile, and the passive influence zone is about six times the diameter of the pile. The angle between the failure planes and the horizontal plane is measured approximately three-fourths of the internal friction angle of soil. The edge of the strain wedge formed in front of the pile is an arc, which is slightly different from the straight line as stated in the literature.

3) The depth of the strain wedge could not be identified from the current test setting due to missing information on soil inside deformation. This will be investigated in the future using transparent soil to capture the inside displacement field as well as the surface displacements. In addition, this study uses scaled models. The scale effect will be considered in future study in order to relate the research findings to real practice. However, this study helps to better understand the soil surface behavior around a laterally loaded pile. The test demonstrates that the optical setup and the stereo-PIV method are suitable for modeling soil-structural interaction problems.

Acknowledgements

The authors acknowledge the China Scholarship Council for the scholarship awarded to the first author during his two-year study at University of Toronto and Ryerson University. The help from Dr. Jinyuan LIU of Ryerson University and Dr. Kaiwen XIA of University of Toronto would also be greatly appreciated.

References

[1] ADRIAN R J. Scattering particle characteristics and their effect on pulsed laser measurements of fluid flow: Speckle velocimetry vs. particle image velocimetry [J]. Applied Optics, 1984, 23(11): 1690–1691.

[2] ELSAYED O A, KWON K, ASRAR W, OMAR A A. Induced rolling moment for NACA4412 plain and flapped wing [J]. Aircraft Engineering and Aerospace Technology, 2010, 82(1): 23–31.

[3] BARNETT C M, BENGOUGH A G, McKENZIE B M. Quantitative image analysis of earthworm-mediated soil displacement [J]. Biology and Fertility of Soils, 2009, 45(8): 821–828.

[4] BENGOUGH A G, HANS J, BRANSBY M F, VALENTINE T A. PIV as a method for quantifying root cell growth and particle displacement in confocal images [J]. Microscopy Research and Technique, 2010, 73(1): 27–36.

[5] ISKANDER M, LIU J. Spatial deformation measurement using transparent soil [J]. Geotechnical Testing Journal, 2010, 33(4): 1–8.

[6] HAJIALILUE-BONAB M, AZARNYA-HAHGOLI H, SOJOUDI Y. Soil deformation pattern around laterally loaded piles [J].

International Journal of Physical Modelling in Geotechnics, 2011, 11(3): 116–125.

[7] XU Jin-ming, CHENG Chang-hong, LU Hai-ping. Strain field investigation of limestone specimen under uniaxial compression loads using particle image velocimetry [J]. Journal of Central South University of Technology, 2011, 18(5): 1619–1625.

[8] CHEUK C Y, WHITE D J, BOLTON M D. Uplift mechanisms of pipes buried in sand [J]. Journal of Geotechnical and Geoenvironmental Engineering, 2008, 134(2): 154–163.

[9] TAYLOR R N, GRANT R J, ROBSON S, KUWANO J. An image analysis system for determining plane and 3-D displacements in soil models [C]// Proceedings of Centrifuge. Balkema, Rotterdam. 1998: 73–78.

[10] VIKRANT T, MICHAEL S, MCNEILL A S R. XU Shao-wen, DENG Xiao-min, FOURNEY W L, DAMIEN B. Application of 3D image correlation for full-field transient plate deformation measurements during blast loading [J]. International Journal of Impact Engineering, 2009, 36(6): 862–874.

[11] BROMS B. Lateral resistance of piles in cohesiveless soils [J]. Journal of the Soil Mechanics and Foundations Division, 1964, 90(SM3): 123–156.

[12] REESE L C. Laterally loaded piles: program documentation [J]. Journal of the Geotechnical Engineering Division-ASCE, 1978, 104(12): 1518–1520.

[13] ASHOUR M, NORRIS G, PILLING P. Strain wedge model capability of analyzing the behavior of laterally loaded isolated piles, drilled shafts and pile groups [J]. Journal of Bridge Engineering, 2002, 7(4): 245–254.

[14] SADEK S, ISKANDER M, LIU Jin-yuan. Accuracy of digital image correlation for measuring deformations in transparent media [J]. Journal of Computing in Civil Engineering, 2003, 17(2): 88–96.

[15] LIU J, ISKANDER M. Adaptive cross correlation for imaging displacements in soils [J]. Journal of Computing in Civil Engineering, 2004, 18(1): 46–57.

[16] ZHANG S, YAU S T. Three-dimensional shape measurement using a structured light system with dual cameras [J]. Optical Engineering, 2008, 47(1): 1–12.

[17] BOUGUET J Y. Camera calibration toolbox for MATLAB [EB/OL]. [2012–03–23]. www.vision.caltech.edu/bouguetj/calib_doc/.

[18] PIVTEC. PIV view user manual [EB/OL]. [2012–03–23]. www.pivtec.com/.

[19] LIU J, ISKANDER M. Modelling capacity of transparent soil [J]. Canadian Geotechnical Journal, 2010, 47(4): 451–460.

[20] LIU J, Yuan Bing-xiang, MAI V, DIMAANO R. Optical measurement of sand deformation around a laterally loaded pile [J]. Journal of Testing and Evaluation, 2011, 39(5): 1–6.

(Edited by DENG Lü-xiang)